Article

Headgroup Percolation and Collapse of Condensed Langmuir Monolayers

Ajaykumar Gopal, and Ka Yee C. Lee

More About This Article

Additional resources and features associated with this article are available within the HTML version:

- Supporting Information
- Links to the 2 articles that cite this article, as of the time of this article download
- Access to high resolution figures
- Links to articles and content related to this article
- Copyright permission to reproduce figures and/or text from this article

View the Full Text HTML

Headgroup Percolation and Collapse of Condensed Langmuir Monolayers[†]

Ajaykumar Gopal* and Ka Yee C. Lee

*Department of Chemistry, the Institute for Biophysical Dynamics, and the James Franck Institute,
The University of Chicago, 5735 S Ellis Avenue, Chicago, Illinois 60637*

Received: March 14, 2006; In Final Form: June 1, 2006

We present a study of Langmuir isotherms and 2D bulk moduli of binary lipid mixtures, where changes in monolayer collapse pressure (Π_c) are followed while varying the relative amounts of the two components. For monolayers containing dipalmitoylphosphocholine (DPPC) with either hexadecanol (HD) or palmitic acid (PA), a distinctly non-monotonic change in Π_c is observed with varying composition. At low mole fractions, there is a slight decrease in Π_c as films get richer in DPPC, while a sharp increase to pure DPPC-like values is observed when the mole fraction exceeds ~0.7. The sudden transition in collapse pressure is explained using the principles of rigidity percolation, and important ramifications of this phenomenon for biological surfactant are discussed.

1. Introduction

Langmuir monolayers provide a unique way of studying two-dimensional (2D) materials at asymmetric interfaces with control over many experimental parameters such as temperature, composition, packing density, and the interfacial environment.[1] Depending on the nature of the amphiphile, physical properties of monolayers at the liquid–gas interface are of great interest from fundamental, materials, and, more recently, biological perspectives.[2–5] In particular, the study of monolayer collapse (how a film, compressed to the limit of its stability in two dimensions, explores the third) gives us insight into the origin and nature of defects in films such as those that coat optical fibers[6,7] and biological ones that protect the eyes,[8,9] ears,[10,11] or the inner surface of our lungs.[12–14]

A lot is already known about polymorphism and two-dimensional phase transitions in Langmuir monolayers.[2,3,15,16] Over the past few years, the evolution of sophisticated Langmuir trough designs that can sustain high surface pressures (Π) and allow concurrent microscopic visualization has enabled several studies of the morphology of collapsed structures formed from highly compressed monolayers. Notably, laser light scattering,[17,18] fluorescence,[19] and Brewster angle microscopy[20–22] of single- and multicomponent polymeric and biological amphiphiles have revealed nano-, micro-, and millimeter scaled collapsed structures.[23–28] In general, it is seen that condensed (solidlike) monolayers collapse by forming either anisotropic crystals or cracks and folds directed perpendicular to the direction of compression. In contrast, liquid monolayers form local axisymmetric defects by budding of tubes, disks, and vesicle-like structures.[29] Concurrently, theories that compare the collapsing monolayer to a 2D material with nucleation and growth of a 3D phase,[30,31] a viscoelastic sheet,[32] an elastic cracking material,[18] or one where the morphology stabilizes topographic features[33,34] have been suggested.

In this study, we neither investigate collapse morphology nor propose a new theory to interpret these structures. Instead, we ask whether the maximum surface pressure (Π_c) sustained by a monolayer prior to collapse can be determined from its composition. In other words, for a simple two-component miscible system where the collapse pressures of the individual components are significantly different, how does the collapse pressure change when the relative amounts of the two are varied?

Since readily available insoluble surfactants which collapse as liquid monolayers were found not to offer sufficiently different collapse pressures, the surfactants chosen for this study collapse from a condensed state (characterized by the ordering in their hydrocarbon tails). Further, we have chosen molecules bearing hydrocarbon tails of identical length so that we can focus on the effects of the headgroup, something not easily studied even by the latest high-resolution synchrotron-radiation-based techniques.[15] Our first molecule of choice is dipalmitoylphosphocholine (DPPC), the predominant lipid component of lung surfactant,[35,36] which has one of the highest collapse pressures reported ($\Pi_c \sim 70$ mN/m) and an extensively studied phase diagram.[37,38] The second component chosen, also containing 16-C hydrocarbon tails, is either 1-hexadecanol (HD, $\Pi_c \sim 60$ mN/m) or palmitic acid (PA, $\Pi_c \sim 40$ mN/m). For both HD: DPPC and PA:DPPC mixtures, at least 13 different stoichiometries were studied, allowing a wide range of DPPC mole fractions (χ_{DPPC}). Moreover, for some of these mixtures, we have already studied the nature of tail ordering in condensed films prior to collapse,[39] allowing better molecular interpretation of collapse pressures. The current work reveals that the above systems show a curiously non-monotonic change in collapse pressure as a function of χ_{DPPC}. In addition, the vital role of headgroups in determining the above behavior is confirmed using studies of dipalmitoylphosphoglycerol (DPPG) monolayer collapse.

The ensuing section lists relevant materials and methods. It is followed by experimental results consisting of surface pressure versus area (Π–A) isotherms and 2D bulk modulus (Π–β) profiles for the individual lipids and their mixtures. Finally, we discuss the trends in collapse pressure with change in composition and relate these to a simplified physical model invoking rigidity percolation.

2. Materials and Methods

2.1. Isotherm Data Collection and Lipids. 1,2-Dipalmitoyl-*sn*-glycero-3-phosphocholine (DPPC, >99%) and the sodium

* Corresponding author. Present address: UCLA Department of Chemistry, 607 Charles E. Young Drive East, Los Angeles, CA 90095. E-mail: agopal@chem.ucla.edu.

salt of 1,2-dipalmitoyl-*sn*-glycero-3-[phospho-rac-(1-glycerol)] (DPPG, >99%) were obtained from Avanti Polar Lipids (Alabaster, AL). Palmitic acid (PA, 99%) was obtained from Aldrich Chemicals (Milwaukee, MO) and 1-hexadecanol (HD, >99%) from Fluka (Milwaukee, MO). All lipids were dissolved in chloroform (HPLC grade, Fisher Scientific, Hampton, NH) and diluted to 0.1 mg mL^{-1} before they were spread at the air–water interface. A few drops of methanol (HPLC grade, Fisher Scientific, Hampton, NH) were used to aid dissolution of DPPG into chloroform. The subphase for all the experiments contained ultrapure water (resistivity ≥18 MΩ cm) made using a combination of reverse osmosis and ultrapurification (RiOs/Elix-10 and Milli-Q, Millipore, Bedford, MA). For some DPPG experiments, sodium chloride (NaCl, SigmaUltra grade, Sigma-Aldrich Corp., St. Louis, MO) and calcium chloride (CaCl$_2$, certified ACS grade, Fisher Scientific, Hampton, NH) were also added to the subphase. Surface pressure versus area (Π–A) isotherms were obtained using a home-built Langmuir trough[19] by monitoring the surface pressure with a Wilhelmy surface balance (Reigler & Kirstein, Berlin, Germany) as the surface area was reduced (compression) or increased (expansion). The instrumentation is detailed elsewhere[26,29,40] and summarized below. The apparatus consists of a Teflon trough (27.5 cm × 6.35 cm × 0.63 cm) fitted with two symmetrically mobile barriers (*l* = 6.35 cm) made of the same material and a filter-paper strip used as the surface balance probe. The maximum working surface area is 145 cm^2. The isotherms for the HD:DPPC and PA:DPPC systems are collected at a linear compression rate of 0.2 mm s^{-1}. Depending on the initial amount of material deposited at the interface, this translates to a molecular area reduction rate between 0.08 and 0.12 Å^2 s^{-1}. Half the above compression rate (0.1 mm s^{-1}) is used for the DPPG experiments (as discussed later, a factor of 2 difference in compression rate is not expected to lead to significant differences in collapse behavior). Monolayers of varying composition, for a given system, are spread at similar initial mean molecular areas (120 ± 5 Å^2 for HD:DPPC, 70 ± 5 and 130 ± 15 Å^2 for PA:DPPC, and 127 ± 2 Å^2 for DPPG). The temperature of the aqueous subphase is maintained within 0.5 °C of the target temperature (30 °C for mixed systems and 25 °C for DPPG films) using a home-built control assembly consisting of thermoelectric units (Omega Engineering Inc, Stamford, CT) attached to a heat sink maintained at 20 °C by a Neslab RTE-100 water circulator (Portsmouth, NH).

2.2. Compressibility and Monolayer Transitions. Whether the ability of the film to store mechanical energy as stress (i.e., its bulk modulus) prior to collapse captures the trends in collapse pressure is an important question. We address this by evaluating the pseudoequilibrium 2D bulk modulus profiles computed from isotherm data.

For a 3D material at equilibrium, one can define the isothermal bulk modulus of a material as

$$\beta_T = -V\left(\frac{\partial P}{\partial V}\right)_T \tag{1}$$

Similarly, one can define an effective 2D isothermal bulk modulus for monolayers as

$$\beta = -A\left(\frac{\partial \Pi}{\partial A}\right)_T \tag{2}$$

the inverse of which yields the isothermal 2D compressibility (κ) of the film

$$\kappa = \frac{1}{\beta} = -\frac{1}{A}\left(\frac{\partial A}{\partial \Pi}\right)_T \tag{3}$$

Being second derivatives of the surface free energy with respect to area, β and κ are expected to show discontinuities during both first- and second-order transitions. This is used for confirming the presence of phase transitions as well as the miscibility of components.

The compressibility of an ideal monolayer containing more than one component can be expressed in terms of its composition and the partial molar areas of its components[41] in the form

$$\kappa = \sum_i R_i(a^i_\rho, \chi^i, \chi_0)\frac{\partial \chi^i}{\partial \Pi} + \sum_\rho \sum_i S_i(a^i_\rho, \chi^i, \chi_0)\frac{\partial a^i_\rho}{\partial \Pi} \tag{4}$$

where (a) the first sum extends over all *i* phases, with χ being the mole fraction, and (b) the second term sums over all *i* phases and components (represented by their packing density (ρ)), with *a* being the partial molar area. *R* and *S* are constants for a given phase.

Monolayers are typically spread at high molecular area in the gas–liquid (G–L) coexistence region. Compression leads to the formation of an isotropic miscible 2D liquid phase marked by an increase in β. This is followed by the onset of the first-order liquid-to-condensed (L–C) phase transition, for which we expect $\partial \chi^i/\partial \Pi$ to go from zero in the homogeneous phase to a finite value in the coexistence region, thus invoking a nonzero first term in eq 4 and leading to a discontinuity in κ and β. A finite compression rate during experiments, however, means that the coexistence region is transgressed under varying pressure. This manifests as a nonhorizontal region in the isotherm and hence a blunt dip instead of a sharp discontinuity in the Π–β plot. Along similar lines, collapse marks the final transition (first-order-like from 2D to 3D) in a monolayer under compression and is accompanied by a corresponding discontinuity in β. Experimentally, this is not found to be a sharp transition either. We therefore report the collapse surface pressure (Π$_c$) as that at which the compressive bulk modulus of the 2D film drops to an arbitrary value of 25 mN/m.

At a surface pressure of 52 mN/m, Teflon is expected to undergo a wetting transition. Due to this, the meniscus of the subphase changes from convex to concave (sometimes called "creepage"). In our experimental setup, the physical dimensions of the monolayer, when it is close to collapse, are considerably small, making it sensitive to perimeter effects. The change in meniscus leads to a non-monotonic error in area during compression, which manifests as a shoulder centered around Π ∼ 52 mN/m and a corresponding drop in β between 50 and 60 mN/m. This phenomenon is commonly reported in the literature and recognized as an artifact of the Langmuir trough for high-surface-pressure studies (for examples, see refs 23 and 42). The prominence of the shoulder depends on the perimeter-to-area ratio of the trough when the film reaches the said pressure range, and is sensitive to compression rate. Despite this error introduced in *A* values at high pressure, the measured values of Π are accurate at collapse. Captive bubble isotherm measurements for DPPC,[43] where the surfactant is confined at a spherical interface instead of a rectangular trough, confirm that the shoulder disappears while retaining the expected collapse pressure.

2.3. Data Processing and Digitization. The Π and *A* values during each experiment are sampled at 1 Hz and output as a digital isotherm file containing a sequential array of instantaneous data. The derivative curves required for computing the

Collapse of Condensed Langmuir Monolayers

J. Phys. Chem. B, Vol. 110, No. 44, 2006 **22081**
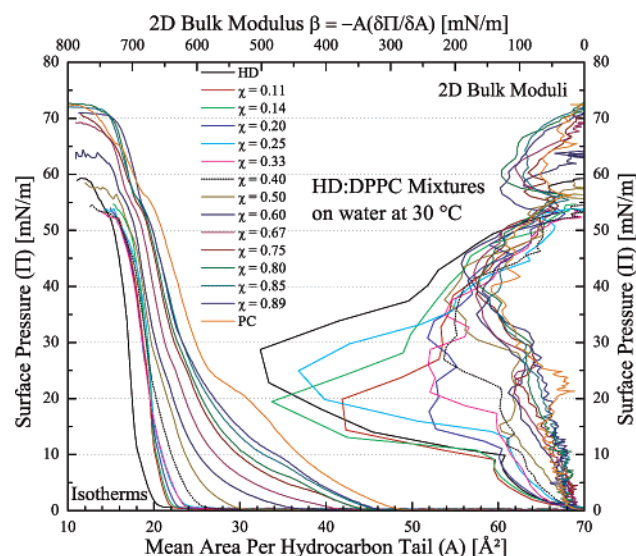
Figure 1. Hexadecanol:DPPC mixtures at 30 °C, with $\Pi-A$ and $\Pi-\beta$ profiles for 15 stoichiometries, showing β on the upper *x*-axis. The isotherm for HD is shifted to the left by 2 Å^2 for easy viewing. Isotherms and bulk moduli are shown with consistent color coding (in the legend, $\chi = \chi_{DPPC}$ and PC = DPPC).

bulk modulus profiles are obtained by calculating the slope (*m*) at each point using the coordinates of two neighboring points and the formula

$$m(x_i, y_i) = \frac{1}{2}\left(\frac{y_{i+1} - y_i}{x_{i+1} - x_i} + \frac{y_i - y_{i-1}}{x_i - x_{i-1}}\right) \qquad (5)$$

DPPG derivative curves (isotherm data obtained at a lower rate of compression) exhibit a high-frequency, low-amplitude noise arising from fluctuations in the surface pressure readings due to discretization and environmental factors. This noise is safely suppressed using a Fourier smoothing filter which removes components with frequencies higher than the cutoff value $1/n\Delta t$ for an assigned value of *n* consecutive data points ($\Delta t = 1$ s). A parabolic function with its maximum at zero frequency and falling to zero at the cutoff is used for this clipping. In the case of DPPG, optimal noise removal is achieved using $n = 20$. The isotherm derivatives for systems containing DPPC with HD or PA do not require Fourier filtering and are used as-is to compute the bulk modulus profiles. $\Pi-\beta$ profiles are shown using the top and right axes where relevant.

The derivative and Fourier filtering tools detailed above are both built-in functions available through the graphing software used for analysis, Origin 6.1 (OriginLab Corp., Northampton, MA). The open-source Engauge Digitizer[44] software is used to digitize Π_c data from studies published by other groups.

3. Results

Figure 1 shows isotherm data and associated $\Pi-\beta$ curves for HD, DPPC, and thirteen HD:DPPC mixtures, representing fifteen different stoichiometries. The isotherm for HD has been offset to the left by 2 Å^2 to help differentiate HD from the rest of the curves clustered in the same region; this should not affect the corresponding $\Pi-\beta$ profile. Since the individual hydrocarbon tails in DPPC and HD are identical, the values of *A* for this system have been normalized to depict the mean surface area per hydrocarbon tail. The main trends in the data are enumerated below.

(1) At 30 °C, HD is below its triple point for the coexistence of the G, L, and C phases. As a result, the film exhibits G–C

coexistence at high *A* and the surface pressure lifts off when the condensed domains contact each other. The kink in the isotherm and the associated kink in the $\Pi-\beta$ profile ($\Pi \sim 10$ mN/m) are due to an order–disorder transition between condensed phases often observed in single chain fatty acids and alcohols.[41,45] GIXD measurements conducted in our earlier study[39] at $\Pi = 15$ mN/m indicate that the phase resulting from this transition showed $\leq 5°$ tilt of the hydrocarbon tail from the surface normal and a projected area per tail of 20.28 Å^2.

As DPPC is added to HD, up to $\chi_{DPPC} = 0.5$, the position of the kink in the isotherm occurs at around the same area per tail (20–21 Å^2). At the same time, the corresponding surface pressure gradually increases from ~ 10 to ~ 28 mN/m, until χ_{DPPC} exceeds 0.5. As mixtures are made richer in DPPC, the kink moves to higher *A* values. In this regime, the expected discontinuity in the $\Pi-\beta$ profile is very subtle and appears as a small bump, hard to discern from the noise (the transition is also confirmed in the $\beta-A$ profiles, not shown). For DPPC-rich mixtures, the highest pressure for this transition is around 32 mN/m, for a $\chi_{DPPC} = 0.89$ monolayer.

(2) The L–C phase transition and the resulting coexistence region for DPPC at 30 °C occur between surface pressures of 18 and 26 mN/m. This corresponds to a broad shoulder in the isotherm and a dip in β. With the addition of HD, the shoulder gets narrower and occurs at lower values of Π. This behavior reaches its limit for $\chi_{DPPC} = 0.6$, where the coexistence plateau is undetectable. This is corroborated by (i) the lack of corresponding features in the $\Pi-\beta$ profile and (ii) our earlier fluorescence data[39] for $\chi_{DPPC} < 0.6$ monolayers, which indicate no L phase and a fully condensed film at $\Pi > 5$ mN/m.

(3) At collapse, there is material lost from the 2D interface, and as expected, the isotherms show a horizontal plateau and the bulk modulus drops to near-zero values. When DPPC is added to HD, the collapse pressure (59 mN/m for pure HD) drops to the range 52–55 mN/m for $\chi_{DPPC} \leq 0.4$. Further addition of DPPC leads to a rapid increase in the collapse pressure, and mixtures with $\chi_{DPPC} > 0.7$ show a collapse pressure indistinguishable from that of DPPC. This non-monotonic trend is visible in the isotherms as well as the $\Pi-\beta$ profiles. A plot of Π_c as a function of χ_{DPPC} is shown in Figure 3 (squares) to clearly illustrate the same.

It is also worth noting that collapse occurs in a narrow range of mean projected tail areas between 17 and 19 Å^2 for all of the films above. It is implicit that all monolayers are in a condensed state prior to collapse.

Similarly, isotherms and $\Pi-\beta$ profiles were determined for PA, DPPC and eleven PA:DPPC mixtures, representing thirteen different stoichiometries. These films behave qualitatively similar to mixed HD:DPPC monolayers. As seen in Figure 2, the rapid increase in collapse pressure again occurs at $\chi_{DPPC} > 0.5$, and for $\chi_{DPPC} > 0.7$ the collapse pressures are, within experimental error, identical to that for pure DPPC (~ 70 mN/m). The films in Figure 2 were spread at a lower initial area per molecule (70 ± 5 Å^2) to verify that the collapse plateaus persist upon compression beyond collapse. Another set of films spread at a higher initial area per molecule of 130 ± 15 Å^2 (isotherms provided as Supporting Information) yielded experimentally indistinguishable collapse pressures. The collapse data obtained from the latter set are reported in Figure 3 (circles) for comparison with the HD:DPPC system (squares). Similar qualitative behavior between HD:DPPC and PA:DPPC systems is clearly seen through the entire range of mixed lipids. The only significant difference in the Π_c values between the two
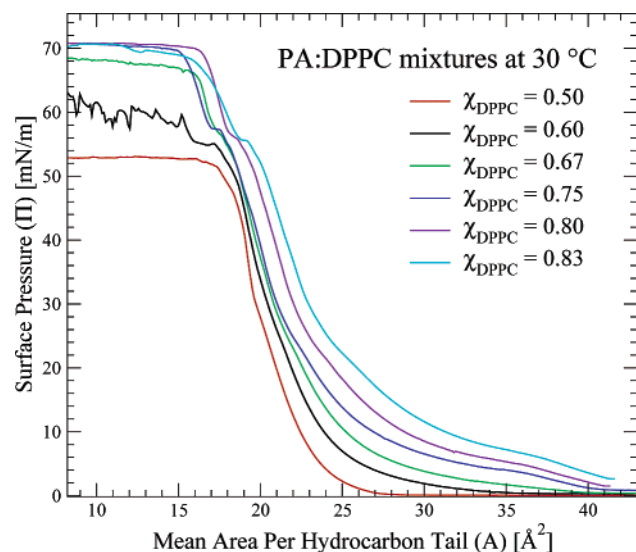
Figure 2. PA:DPPC mixtures at 30 °C at the air−water interface. For simplicity, isotherm data for only 6 of the 13 stoichiometries measured are shown. The collapse plateau for all of these films occurs at $A < 20$ Å².
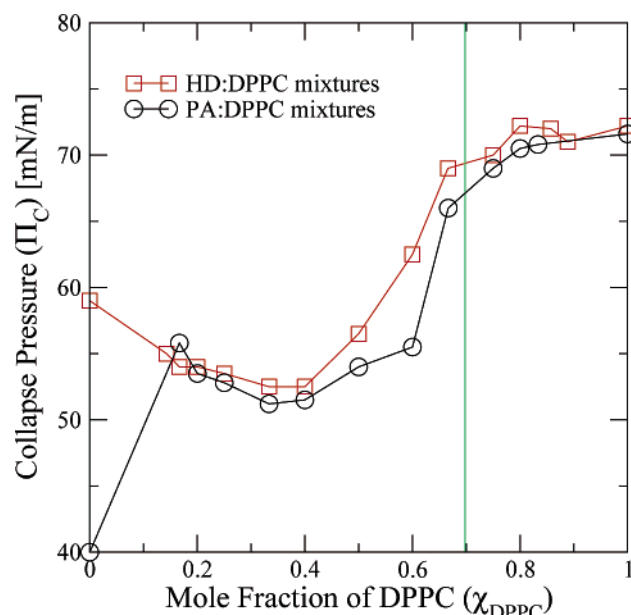
Figure 3. Collapse pressure (Π_c) vs χ_{DPPC}, the mole fraction of DPPC, in mixed monolayers containing HD:DPPC and PA:DPPC. The green line indicates the rigidity site percolation threshold $\chi_{DPPC} = q^\star \approx 0.7$.

systems occurs for the single-component HD and PA monolayers (i.e., $\chi_{DPPC} = 0$).

Figure 4 shows isotherms and $\Pi-\beta$ profiles for DPPG monolayers spread on three different subphases: deionized water, 150 mM NaCl, and 5 mM $CaCl_2$ + 150 mM NaCl. The addition of NaCl (red curve) to a water subphase (black curve) causes a drastic change in the DPPG isotherm, which shifts to the right and shows a pronounced L−C coexistence plateau resembling DPPC. Accordingly, the collapse pressure of the monolayer increases from ∼55 to ∼71 mN/m. Further addition of 5 mM Ca^{2+} ions (green curve) shifts the isotherm back to the left, removes the L−C plateau, and reduces the collapse pressure to an intermediate value of ∼62 mN/m. It is interesting to note that the highest β values during compression were observed when pure water was used as the subphase.
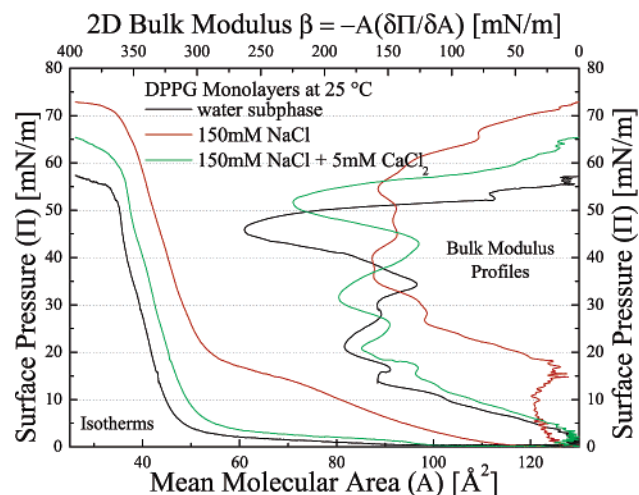

Figure 4. $\Pi-A$ isotherms and $\Pi-\beta$ profiles for DPPG monolayers at 25 °C spread on three different subphases. The collapse pressures (Π at $\beta = 25$ mN/m) are, respectively, 55, 62, and 71 for DPPG on pure (i) water, (ii) 5 mM $CaCl_2$ + 150 mM NaCl, and (iii) 150 mM NaCl. Since all three monolayers are the same molecular species, the isotherms are presented in terms of the mean molecular area. Mean areas per hydrocarbon tail (used in Figures 1 and 2) can be obtained by halving these values.

4. Discussion

From the above results, we notice that, for HD-rich monolayers ($\chi_{DPPC} < 0.5$), the order−disorder transition kink occurred around the same value, $A \sim 20$ Å². (Recall that the HD isotherm has been offset to the left by 2 Å².) In the case of a $\chi_{DPPC} = 0.5$ HD:DPPC mixture, the kink in the isotherm was found at $\Pi = 28$ mN/m. At this pressure, one would expect pure DPPC and HD monolayers to individually be in the C phase with $A \sim 26$ and 20 Å², respectively. The negative deviation of the tail area for the $\chi_{DPPC} = 0.5$ mixture from the expected mean of its components suggests that the two components mix nonideally. Moreover, all condensed films with $\chi_{DPPC} > 0.5$ show an increase in A at $\Pi = 30$. This, and the presence of L−C phase coexistence in films with $\chi_{DPPC} > 0.67$ at lower surface pressure, indicate that DPPC-rich mixtures increasingly behave like pure DPPC. However, as seen in Figure 3, the collapse pressures of DPPC-rich films do not show a gradual increase from 55 to 70 mN/m as one would expect. To understand this phenomenon, we first describe the molecular ordering in these films in their condensed state at $\Pi = 40$ mN/m.

In an earlier grazing-incidence X-ray diffraction (GIXD) study of HD:DPPC and PA:DPPC mixtures, we have shown that both HD and PA form miscible condensed "alloys" with DPPC at an optimal stoichiometry of 1:1[39] ($\chi_{DPPC} = 0.5$). In particular, at $\Pi = 40$ mN/m, HD- or PA-rich mixtures up to $\chi_{DPPC} = 0.5$ show a single diffraction peak at $A \sim 20$ Å² with chain tilt angles of <5° to the surface normal, indicating the presence of vertically oriented tail groups on a triangular lattice (sometimes called hexagonal order). For DPPC-rich films, one finds gradual deviation of the monolayer order from a purely hexagonal packing to one that includes rectangular unit cells (revealed by the presence of more than one Bragg peak). Monolayers of $\chi_{DPPC} = 0.75$ HD:DPPC, for example, reveal two unit cells using GIXD: one identical to the untilted 1:1 alloy mentioned above and the other, with the hydrocarbon chains tilted at 19.1°, similar to the tilted condensed phase observed in pure DPPC monolayers.

The tilting of tails in a condensed DPPC monolayer arises due to the projected headgroup area of DPPC being large relative
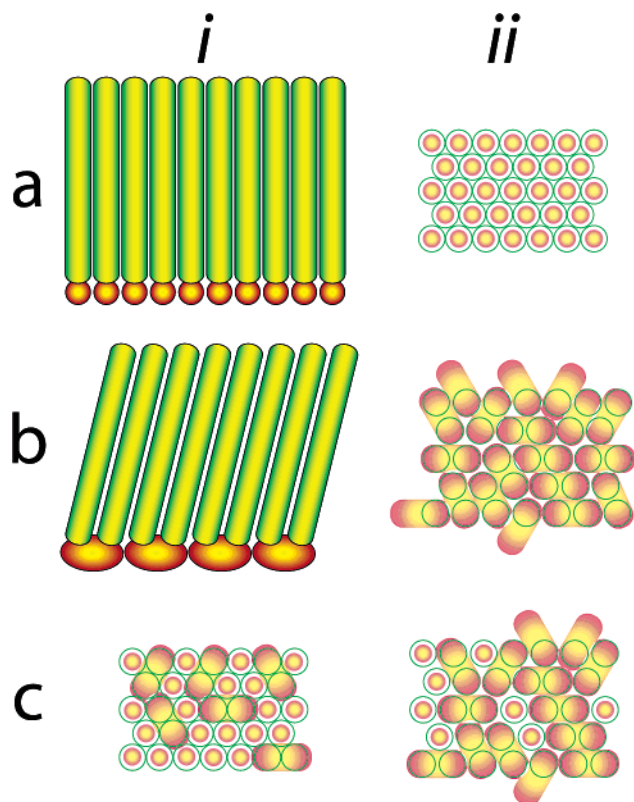
Figure 5. Schematic representation of relative projected areas and packing of headgroups (orange spheres and ellipsoids) and tails (green rods and circles). Part a-i,ii shows the side and bottom-up projected view of a HD monolayer, where the headgroup projected area is smaller than that of the tail. Similarly, part b-i,ii shows views of a DPPC monolayer where the headgroup projected area is larger than that of the tails, leading to a tilted condensed phase (denoted by gaps between green circles in the projection). Despite the presence of ordered tail groups in a regular triangular lattice, the headgroups form a random lattice. The DPPC headgroups are drawn as ellipsoids to illustrate that each headgroup is associated with two tails; they are considered as randomly packed spheres in the text. Parts c-i and c-ii represent projections of mixed HD:DPPC films at concentrations where percolation of large DPPC headgroups is, respectively, absent or present.

to that of an untilted tail[15] (see Figure 5a,b). Tilting allows the tails to maximize Van der Waals interactions in the limit where the bulky headgroup does not allow the proximity required for hexagonal packing. In contrast, pure HD and PA monolayers show hexagonal ordering of hydrocarbon tails, indicating headgroups whose projected areas are effectively similar to, if not smaller than, that for the 16-C tail. Along the same lines, mixing lipids bearing smaller headgroups such as HD or PA with DPPC reduces the mean projected headgroup area relative to the tails, allowing hexagonal packing. One can easily infer the relative headgroup sizes (projected areas) of the two lipids from the optimal stoichiometry (1:1), knowing that the tails are identical and hexagonally ordered.

With this knowledge, we now address the main question posed by this study, which, in the current context, can be stated as follows: At what value of χ_{DPPC} does the mixed monolayer collapse at a pressure indistinguishable from pure DPPC, and why? From Figure 3, we know that the answer is nontrivial because mixed HP:DPPC and PA:DPPC monolayers with $\chi_{DPPC} \geq 0.7$ collapse at almost the same pressure as DPPC. Using the ensuing model based on rigidity percolation, we show that lateral connectivity between the large DPPC headgroups is sufficient to explain the above phenomenon.

4.1. Rigidity Percolation Treatment. Percolation theory[46,47] primarily deals with the existence of a connected pathway in lattices whose sites (or bonds) are occupied to different extents. The site percolation threshold ($q^\star$) for a 2D lattice is the fraction (*f*) of lattice sites that needs to be randomly populated until a nearest-neighbor connected cluster spans the entire lattice. The concept of rigidity percolation[48] further extends this idea to vectorial long-range connectivities for estimating the probability of forming not only a spanning cluster but also one that is rigid with respect to applied forces. Next, we map the concepts of 2D rigidity percolation to our composition-collapse problem.

Let us consider a pure DPPC monolayer compressed to a molecular area approaching collapse (say the point when $\Pi = 50$ mN/m). Microscopically, this represents a polycrystalline (2D powderlike) condensed phase with rectangular unit cells of tilted tails having a lateral correlation length of the order of 10 s of intermolecular distances.[39] Despite the order in the tail regions, there are many degenerate headgroup configurations associated with a condensed domain, since two tails are bound to each headgroup.[15] Moreover, the headgroups are asymmetric and possess rotational freedom, leaving even the tail-ordered regions of the monolayer with essentially no translational or orientational headgroup order. Considering the fact that the macroscopic monolayer is made up of such microscopic regions separated by grain boundaries, one expects very little correlation between the positions and orientations of the headgroups in a condensed film. Since (bulky) headgroups determine the projected area of a DPPC monolayer, we equate the formation of a condensed monolayer to the formation of a random close-packed 2D lattice of headgroups (assumed to be spherical for simplicity). In this scenario, a pure DPPC monolayer is equivalent to a rigid and fully percolated generic 2D lattice[48] of headgroups (instead of a regular lattice of tails), where the fraction of sites occupied is essentially unity (Figure 5b-ii). This picture can now be extended to mixed monolayers, where a reduction in χ_{DPPC} is identical to a dilution (i.e., $f < 1$) of the generic 2D lattice, with the empty sites representing much smaller PA or HD headgroups (Figure 5c-ii). The minimum value of χ_{DPPC} for which the monolayer can have the same collapse pressure as DPPC thus becomes the rigidity site percolation threshold for the generic 2D lattice.

Jacobs and Thorpe[49] have estimated $q^\star$ for a generic 2D lattice at 0.69755 ± 0.0003. The minimum χ_{DPPC} for a mixed monolayer to exhibit DPPC-like collapse is, therefore, expected when $\chi_{DPPC} = q^\star \approx 0.7$. A mixed monolayer of this composition, in theory, should be critically rigid (i.e., containing a single spanning cluster with no redundant constraints). The statistical probability of forming a critical cluster at $f = q^\star$ is reported to be around 0.9.[49] Since the configuration of the cluster would be different for each trial, its stability toward finite shear or lateral stresses is also expected to vary. Experimentally, it follows from the above that monolayers with overconstrained clusters (i.e., χ_{DPPC} slightly higher than $q^\star$) should behave more reliably like the pure component than a monolayer with $\chi_{DPPC} = q^\star$.

Figure 3 confirms that the steepest increase in Π_c for mixed monolayers containing DPPC and HD or PA occurs as the threshold composition is approached; that is, χ_{DPPC} is raised from 0.6 to 0.67 in our experiments. Values of Π_c for monolayers above the threshold composition, that is, with $\chi_{DPPC} \geq 0.75$, are practically indistinguishable from that of pure DPPC.

Since this result primarily relies on headgroup arrangements, it can be generalized to any monolayer with similar head-to-tail geometries. In particular, it must apply to all mixed
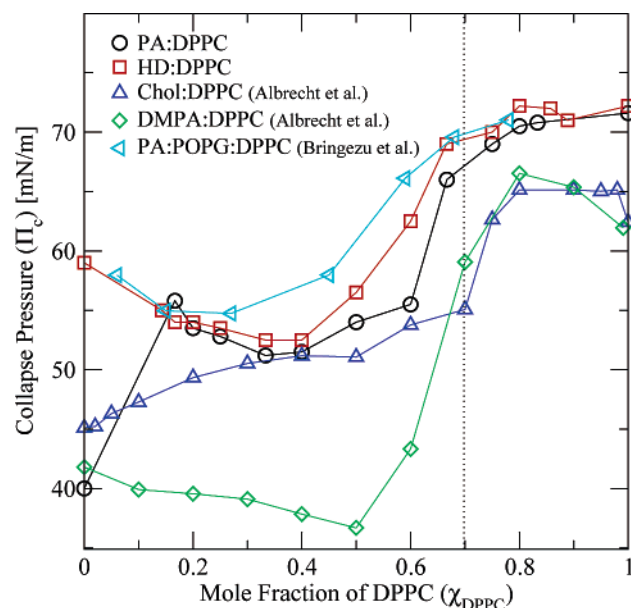
Figure 6. Collapse pressure (Π_c) vs χ_{DPPC}, the mole fraction of DPPC, in various mixed monolayers. The curves for HD:DPPC and PA:DPPC systems are from Figure 3, and the others were digitized from their respective references. The dotted line indicates the rigidity site percolation threshold $\chi_{DPPC} = q^\star \approx 0.7$.

monolayers of DPPC with lipids that contain smaller headgroups and projected tail areas similar to or smaller than DPPC. As reviewed below, this trend is confirmed by several prior studies of collapse as a function of composition, all of which focused on a different problem and did not comment on the sharp transition in collapse pressure. Albrecht et al. have studied the Π versus χ phase diagram for mixtures of cholesterol and DPPC.[41] They report film breakdown pressures close to 50 mN/m for films with $\chi_{DPPC} < 0.6$ and around 62–65 mN/m when $\chi_{DPPC} > 0.7$. In the same paper, collapse pressures for binary DPPC:DMPA (dimyristoylphosphatidic acid) mixtures are reported to increase abruptly from around 40 to over 65 mN/m when χ_{DPPC} is increased from 0.6 to 0.8. More recently, Bringezu et al. have published isotherm, fluorescence and GIXD data for ternary mixtures containing DPPC, POPG (palmitoyloleoylphosphoglycerol), and PA.[50] Mixtures richer in DPPC than a 62/18/20 (w/w/w) mixture of DPPC/POPG/PA are reported to collapse at a surface pressure of nearly 70 mN/m, the value expected for pure DPPC. Figure 6 shows the results of the above studies overlaid on the data from Figure 3. It is clear in the above cases that the transition of collapse pressure from the lower to higher DPPC-like values always occurs at χ_{DPPC} values between 0.6 and 0.8. Although the collapse pressure for the pure DPPC monolayer reported by Albrecht et al.[41] is slightly lower than the more recent studies, it is sufficient to note that the transition to a DPPC-like value still occurs in the range noted above. This seemingly universal trend directly supports our rather simple rigidity percolation treatment. It is expected that slight differences in the position and sharpness of the transition region in a Π_c versus χ_{DPPC} plot will arise from higher order effects such as long-range correlations between headgroup positions, microscopic phase separation, headgroup electrostatics, and the head-to-tail projected area ratios (i.e., spontaneous curvatures) of the components. How these factors may affect the formation of a percolated stress-bearing network and other physical studies to confirm the above model are discussed in the next section.

As χ_{DPPC} is reduced below the threshold concentration, Π_c is expected to fall to a value corresponding to the second

component. Moreover, at a value of χ_{DPPC} below which the mean projected area of headgroups is smaller than that of the tails, Π_c represents the lateral stability of an ordered hydrocarbon monolayer. One would ideally expect no changes in the collapse pressure with further reduction of χ_{DPPC}. In contrast, Figure 3 indicates a small but systematic increase in collapse pressure as χ_{DPPC} is reduced below 0.5. This phenomenon remains an interesting puzzle. A possible explanation lies in the fact that, for most of the mixtures with χ_{DPPC} between 0 and 0.5, the mean area per hydrocarbon tail prior to collapse (say $\Pi = 50$ mN/m) remains unchanged despite the change in composition (described earlier in the Results section). This occurs with no change in the tail order in the system, suggesting that favorable dispersive interactions from vertically oriented hydrocarbon tails may be able to sustain local defects in headgroup packing in the form of bulky headgroups (see 5c-i). Thus, addition of DPPC to a HD monolayer up to $\chi_{DPPC} = 0.5$ represents the formation of tail-ordered monolayers with increasingly frustrated headgroup packing. The decreasing peak β values for these films (Figure 1) and a drop in their collapse pressures are consistent with this interpretation. The increase in collapse pressure and mean area per tail for monolayers with $\chi_{DPPC} \geq 0.5$ may thus represent a steric or geometric transition where dispersive interactions are not able to stabilize a higher surface density of DPPC headgroups. In other words, the mean projected area of the headgroups increases beyond that of a hydrocarbon layer with vertically oriented tails. As noted earlier, monolayers with $\chi_{DPPC} > 0.5$ also display a tilted hydrocarbon tail order besides hexagonal, which is a way for the system to maximize dispersive interactions while reducing steric frustration.

4.2. Other Considerations and Open Questions. Strictly speaking, the proposed model is only valid for completely miscible solid films where one of the molecules has a headgroup with a projected area larger than any of the tails in the mixture. Moreover, since we assume headgroups to be uncharged solid spheres, we do not account for electrostatic, chirality, and hydration effects. In this section, we try to rationalize the effects of these parameters.

Phase Separation. In the event that the components of a condensed film phase-separate during compression, one is left with a heterogeneous film prior to collapse. Depending on the relative solubilities of components, domains of the phase with $\chi_{DPPC} > 0.7$ are expected to be rigid. Separation of phases, therefore, introduces positive correlations in the positions of headgroups of a certain type. In general, this implies an increased probability of finding a similar headgroup as the nearest neighbor, making the formation of a rigid cluster more probable. Ultimately, the relative coverage and morphologies of the rigid and nonrigid phases will govern the collapse pressure of a biphasic film. Along these lines, films forming a sufficiently large coverage of phase-separated domains show correlations between surface rheology and a percolated domain morphology visible by optical microscopy.[51,52]

Tailgroup Effects. When a monolayer contains only lipids with mean projected tail area larger than that of the head (e.g., cholesterol, unsaturated lipids, etc.), headgroup percolation will not play as important a role as tail percolation in determining collapse. Π_c would now become sensitive to both the ordering and the extent of lateral correlation between tails. When such molecules are mixed with DPPC, we expect two regimes of collapse behavior. Mixed films of high DPPC content, due to the large DPPC headgroups and the overall tail cross-sectional area being smaller than that of heads, should allow headgroup percolation and DPPC-like collapse at $\chi_{DPPC} > 0.7$. When the

Collapse of Condensed Langmuir Monolayers

J. Phys. Chem. B, Vol. 110, No. 44, 2006 **22085**

concentration of DPPC falls below a certain limit, the system can transition to tailgroup dominated collapse behavior, where the explicit details of the hydrocarbon layer become important. Some evidence in this direction can be seen as deviation of the χ_{DPPC} versus Π_c profile for monolayers containing significant amounts of cholesterol (blue curve, Figure 6, $\chi_{DPPC} < 0.5$). To account for such tailgroup effects, one would need to recalculate the rigidity percolation threshold taking into account their lateral correlation lengths and local lattice geometries as additional parameters. We are currently working on exhaustive treatments involving both headgroup and tailgroup effects.

Due to their biological significance, the miscibility phase diagrams for phosphocholines (PCs) with both cholesterol and (nearly identical) dihydrocholesterol have been studied in great detail.[53−56] It has been suggested that, for mixed monolayers of cholesterol (or dihydrocholesterol) with PCs, cholesterol is present in the form of a stoichiometric complex with the phospholipid. Depending on the relative amounts of the two components, the complexed material can be found with an excess of uncomplexed DPPC (alpha phase) or cholesterol (beta phase). The transition from the beta to alpha phase, signifying transition from a monolayer with excess cholesterol to one with excess PCs, is expected to occur at $\chi_{DPPC} \sim 0.65$. At this stoichiometry, we expect a transition from tailgroup dominated collapse behavior to one that relies on headgroup percolation. The presence of excess PC headgroups, at $\chi_{DPPC} > 0.65$, inferred from the above studies and optical microscopy[57] is consistent with the rapid increase in collapse pressure seen in cholesterol: DPPC monolayers between $\chi_{DPPC} = 0.6$ and 0.8 (blue curve, Figure 6). Along similar lines, it may be possible to classify tailgroups of the second component (and therefore the molecules themselves) as either "fluidizing" or "condensing" a film of DPPC according to their abilities to, respectively, increase or decrease the threshold composition for DPPC-like collapse from its expected value ($\chi_{DPPC} = q^\star$).

Headgroup Polarity and Electrostatics. An important molecular parameter neglected in the above treatment is headgroup polarity. Long-range electrostatic and dipolar effects are responsible for the modification of interfacial tension[58−61] as well as the typical microscopic discontinuous phase morphology found in some condensed monolayers.[38,62,63] Moreover, for surfactants like PA that are expected to ionize at the interface, the surface charge density of the monolayer is very sensitive to the pH and Debye length of the subphase. Such effects may lead to the drastically different collapse pressures for PA and its most dilute mixture with DPPC ($\chi_{DPPC} = 0.17$) seen in Figure 3.

Recent studies of the effect of monovalent ions[59−61] on charged surfactant monolayers show a non-monotonic electrostatic contribution to (the free energy and hence) the surface tension of the interface. In DPPG or DMPA monolayers,[59,60] for example, there is an increase in the degree of dissociation of the headgroup until the subphase NaCl concentration of 150 mM is reached. This leads to a higher electrostatic contribution to the surface tension and hence higher Π for a given A value. Further addition of salt screens the charges, reducing this contribution and leading to a drop in Π. Charged lipids tend to have a negative spontaneous curvature[64,65] due to the larger projected area of a hydrated (charged) headgroup relative to the tails. With the above factors in mind, we expect that as the subphase concentration of NaCl is increased from zero to 150 mM, a DPPG monolayer would transition from being almost completely uncharged with smaller headgroups to being completely charged with larger hydrated headgroups. In the latter

case, one would expect that headgroup percolation dominates collapse instead of tail percolation.

We have tested DPPG monolayers under three different subphase conditions (Figure 4) to verify if the large headgroup size of a fully ionized monolayer can lead to percolation similar to that proposed for DPPC (Figure 5b). Indeed, when 150 mM NaCl is used as the subphase, the $\Pi-A$ and $\Pi-\beta$ profiles for DPPG monolayers are qualitatively similar to DPPC. When additional divalent ions are added to the subphase (5 mM CaCl$_2$ + 150 mM NaCl), one sees the collapse pressure drop down to a lower value due to reduction in the headgroup size caused by a higher ionic strength and possible counterion condensation. These data show that it is possible to treat electrostatic interactions by calculating their effect on headgroup size, making future percolation treatments possible. To quantitatively predict such effects, more advanced methods that account for the explicit shape and size of headgroups would need to be developed.

Viscoelasticity. Comparing the $\Pi-\beta$ profiles for DPPG (Figure 4) and HD:DPPC mixtures (Figure 1), the peak bulk moduli of monolayers with and without headgroup percolation show a consistent trend. As mentioned above, we expect tail percolation to occur for DPPG monolayers on pure water, and similarly for HD and HD-rich HD:DPPC monolayers up to $\chi_{DPPC} = 0.5$. The peak bulk moduli for these films are consistently higher than those for the corresponding cases where headgroups percolate (i.e., DPPG on 150 mM NaCl and DPPC-rich mixtures of HD:DPPC). This suggests, for a monolayer under compression, the charged DPPG headgroup and the zwitterionic DPPC headgroup both "delay" to a higher surface pressure the ability of the tails to maximize dispersive interactions and form an incompressible hydrocarbon layer. In other words, large headgroups prevent the buildup of stress at low surface pressure by providing a percolating network of regions more compressible than the hydrocarbon layer. This effective "softening" or change in relaxation time may manifest as changes in collapse kinetics. Consistent with the above picture, a recent study of the fracture kinetics of collapsing dipalmitoylphosphatidylserine (DPPS) monolayers[66] reports that the addition of DPPC (in the limited concentration range where collapse occurs by folding) decreases the 3D fold propagation speed.

A possible weakness of the proposed percolation model is that it predicts the presence of rigidity on the basis of a static configuration of headgroups. Although successful for interpreting the effect of composition on collapse, this model is too simplistic to explain the dynamic response of a monolayer, for example, the rise in collapse pressure of monolayers with increasing rate of strain.[67−69] To explain such phenomena, one may need to include dynamic constraints in the lattice-percolation model as recently done for jammed 2D systems.[70] These are interesting directions for future experimental and theoretical efforts.

For the current study, however, we can show that the jump in collapse pressure of a mixed monolayer when χ_{DPPC} exceeds 0.7 is not consistent with a simple strain-rate-based change in viscoelastic material response. As mentioned earlier, the monolayers for each set of experiments were spread at similar initial molecular areas. Thus, at a given value of A in Figure 1, the physical area of the monolayer can vary from that of pure HD to double that value for pure DPPC, with stoichiometry dependent intermediate values for mixtures. The temporal rate of strain of the monolayer ($-(1/A)(dA/dt)$) accordingly varies at most by a factor of 2, decreasing with the addition of DPPC (increasing χ_{DPPC}). Comparison with earlier reports[67−69] suggests

22086 *J. Phys. Chem. B, Vol. 110, No. 44, 2006*

Gopal and Lee

that such a monotonic decrease in strain rate should lead to a gradual drop in collapse pressure. Our data, however, show an unexpectedly sharp increase as films get richer in DPPC (χ_{DPPC} > 0.5), which suggests that, for the data presented, strain-rate effects are negligible compared to headgroup-composition effects. An additional confirmation can be drawn from the PA: DPPC data. The monolayers leading to the isotherms in Figure 2, before compression, had nearly double the surface density (at identical initial physical area) as those leading to the profiles presented in the Supporting Information. It follows that collapse in the former occurs at nearly double the physical area as the latter, leading to half the strain rate. Despite this, no significant differences in collapse pressure can be seen between the two sets of experiments, confirming that the relaxation times for the solidlike films in our study do not vary significantly with small changes in strain rate. Whether larger changes in strain rate (several orders of magnitude) can nullify or enhance headgroup-percolation effects and whether these can be explained by more advanced percolation models remains to be investigated.

At different compositions below the percolation threshold, one still expects rigid clusters; however, these are not large enough to span the entire system.[49] Macroscopically, the presence of these clusters changes the rheology of the monolayer. Recent shear viscosity measurements on polymer films,[71] which successfully explain the rheology of 2D Langmuir monolayers by taking into account the compressibility of the molecular species that percolate, demonstrate that rigidity percolation promises to be a strong tool to bridge the gap between the molecular and material properties of surfactant monolayers.

4.3. Implications for Biological Surfactant. Langmuir monolayers are used as models for membrane bilayers and directly impact the understanding of biological air–water interfaces such as lung surfactant.[72] Over two decades ago, Tanaka et al.[73–75] performed a systematic comparison of in vivo and in vitro surface behavior of mixtures of various lipids found in lung surfactant. They found that lipid mixtures which were able to reduce interfacial surface tension to near-zero values typically contained 70% or more of the large phosphocholine headgroup. With low surface tension being an important property of lung surfactant and basis for designing lung surfactant replacements, many subsequent studies have empirically used a mixture containing 70% DPPC as the model surfactant.

According to our model, monolayers containing 70% or more DPPC are expected to be above the rigidity percolation threshold. It follows that their collapse surface tensions are similar to that of DPPC ($\Pi \sim 70$ mN/m, i.e., surface tension ~ 2 mN/m at 25 °C). Our percolation model therefore provides a rationale for why the 7:3 "magic" DPPC:X lipid ratio extensively used in the literature as model lung surfactant consistently provides favorable surface tension properties in monolayer studies.

5. Conclusions

We have studied the collapse of mixed condensed films of DPPC with other surfactants having smaller effective headgroup sizes at different values of χ_{DPPC}. We show that the jump in collapse pressure to values similar to pure DPPC films at $\chi_{DPPC} \geq 0.7$ can be simply explained by the presence of a stress-bearing DPPC cluster at a stoichiometry predicted by generic 2D rigidity percolation. The efficacy of the magic mole fraction of DPPC or phosphocholine headgroups ($\chi_{DPPC} = 0.7$, or 7:3

ratio of DPPC with other lipids) for model lung surfactant is possibly linked to this phenomenon.

Supporting Information Available: Figures showing isotherms for thirteen PA:DPPC monolayer stoichiometries at 30 °C on a water subphase. This material is available free of charge via the Internet at http://pubs.acs.org.

References and Notes

(1) Gaines, George L., Jr. *Insoluble Monolayers at Liquid–Gas Interfaces*, 1st ed.; Interscience Publishers: New York, 1966.

(2) Albrecht, O.; Gruler, H.; Sackmann, E. *J. Phys.* **1978**, *39*, 301–313.

(3) Andelman, D.; Brochard, F.; Knobler, C.; Rondelez, F. Structures and phase transitions in Langmuir Monolayers. In *Micelles, Membranes, Microemulsions, and Monolayers*, 1st ed.; Ben-Shaul, A., Gelbart, W. M., Roux, D., Eds.; Springer-Verlag: New York, 1994.

(4) Fendler, J. H.; Meldrum, F. C. *Adv. Mater.* **1995**, *7*, 607–632.

(5) Möhwald, H. Phospholipid Monolayers. In *Handbook of Biological Physics: Structure and Dynamics of Membranes*, 1st ed.; Lipowsky, R., Sackmann, E., Eds.; Elsevier Science Ltd.: Amsterdam, The Netherlands, 1995; Vol. 1A.

(6) Flannery, D.; James, S. W.; Tatam, R. P.; Ashwell, G. *J. Opt. Lett.* **1997**, *22*, 567–569.

(7) Flannery, D.; James, S. W.; Tatam, R. P.; Ashwell, G. *J. Appl. Opt.* **1999**, *38*, 7370–7374.

(8) Glasgow, B. J.; Marshall, G.; Gasymov, O. K.; Abduragimov, A. R.; Yusifov, T. N.; Knobler, C. M. *Invest. Ophthalmol. Visual Sci.* **1999**, *40*, 3100–3107.

(9) Greiner, J. V.; Glonek, T.; Korb, D. R.; Booth, R.; Leahy, C. D. *Ophthalmol. Res.* **1996**, *28*, 44–49.

(10) Grace, A.; Kowk, P.; Hawke, M. *Arch. Otolaryngol.* **1987**, *96*, 336–40.

(11) Hills, B. A. *Arch. Otolaryngol.* **1984**, *110*, 3–9.

(12) Veldhuizen, R.; Nag, K.; Orgeig, S.; Possmayer, F. *Biochim. Biophys. Acta* **1998**, *1408*, 90–108.

(13) Yu, S. H.; Possmayer, F. *J. Lipid Res.* **2003**, *44*, 621–629.

(14) Goerke, J. *Biochim. Biophys. Acta* **1974**, *344*, 241–261.

(15) Kaganer, V. M.; Möhwald, H.; Dutta, P. *Rev. Mod. Phys.* **1999**, *71*, 779–819.

(16) Knobler, C. M.; Desai, R. C. *Annu. Rev. Phys. Chem.* **1992**, *43*, 207–236.

(17) Schief, W. R.; Dennis, S. R.; Frey, W.; Vogel, V. *Colloids Surf., A* **2000**, *171*, 75–86.

(18) Lu, W.; Knobler, C. M.; Bruinsma, R. F.; Twardos, M.; Dennin, M. *Phys. Rev. Lett.* **2002**, *89*, 146107-4.

(19) Lipp, M. M.; Lee, K. Y. C.; Zasadzinski, J. A.; Waring, A. J. *Rev. Sci. Instrum.* **1997**, *68*, 2574–2582.

(20) Angelova, A.; Vollhardt, D.; Ionov, R. *J. Phys. Chem.* **1996**, *100*, 10710–10720.

(21) Lu, Z. H.; Nakahara, H. *Chem. Lett.* **1994**, 2005–2008.

(22) Lheveder, C.; Henon, S.; Mercier, R.; Tissot, G.; Fournet, P.; Meunier, J. *Rev. Sci. Instrum.* **1998**, *69*, 1446–1450.

(23) Schief, W. R.; Hall, S. B.; Vogel, V. *Phys. Rev. E* **2000**, *62*, 6831–6837.

(24) Schief, W. R.; Touryan, L.; Hall, S. B.; Vogel, V. *J. Phys. Chem. B* **2000**, *104*, 7388–7393.

(25) Schief, W. R.; Antia, M.; Discher, B. M.; Hall, S. B.; Vogel, V. *Biophys. J.* **2003**, *84*, 3792–3806.

(26) Gopal, A.; Lee, K. Y. C. *J. Phys. Chem. B* **2001**, *105*, 10348–10354.

(27) Hatta, E.; Fischer, T. M. *J. Phys. Chem. B* **2002**, *106*, 589–592.

(28) Ybert, C.; Lu, W.; Möller, G.; Knobler, C. M. *J. Phys. Chem. B* **2002**, *106*, 2004–2008.

Collapse of Condensed Langmuir Monolayers

J. Phys. Chem. B, Vol. 110, No. 44, 2006 **22087**

(29) Gopal, A. The collapse of phospholipid Langmuir monolayers: Implications for biological surfactant, Ph.D. Thesis, The University of Chicago, 2004.

(30) Smith, R. D.; Berg, J. C. *J. Colloid Interface Sci.* **1980**, *74*, 273−86.

(31) Vollhardt, D. *Adv. Colloid Interface Sci.* **1993**, *47*, 1−23.

(32) Kampf, J. P.; Frank, C. W.; Malmström, E. E.; Hawker, C. J. *Science* **1999**, *283*, 1730−1733.

(33) Diamant, H.; Witten, T. A.; Ege, C.; Gopal, A.; Lee, K. Y. C. *Phys. Rev. E* **2001**, *63*, 061602-12.

(34) Diamant, H.; Witten, T. A.; Gopal, A.; Lee, K. Y. C. *Europhys. Lett.* **2000**, *52*, 171.

(35) Kahn, M. C.; Anderson, G. J.; Anyan, W. R.; Hall, S. B. *Am. J. Physiol.* **1995**, *13*, L567−L573.

(36) Bernhard, W.; Hoffmann, S.; Dombrowsky, H.; Rau, G. A.; Kamlage, A.; Kappler, M.; Haitsma, J. J.; Freihorst, J.; von der Hardt, H.; Poets, C. F. *Am. J. Respir. Cell Mol. Biol.* **2001**, *25*, 725−731.

(37) Möhwald, H. *Annu. Rev. Phys. Chem.* **1990**, *41*, 441−476.

(38) McConnell, H. M. *Annu. Rev. Phys. Chem.* **1991**, *42*, 171−195.

(39) Lee, K. Y. C.; Gopal, A.; von Nahmen, A.; Zasadzinski, J. A.; Majewski, J.; Smith, G. S.; Howes, P. B.; Kjaer, K. *J. Chem. Phys.* **2002**, *116*, 774−783.

(40) Lipp, M. M.; Lee, K. Y. C.; Zasadzinski, J. A.; Waring, A. J. *Rev. Sci. Instrum.* **1997**, *68*, 2574.

(41) Albrecht, O.; Gruler, H.; Sackmann, E. *J. Colloid Interface Sci.* **1981**, *79*, 319−338.

(42) Yan, W. F.; Piknova, B.; Hall, S. B. *Biophys. J.* **2005**, *89*, 306−314.

(43) Crane, J. M.; Putz, G.; Hall, S. B. *Biophys. J.* **1999**, *77*, 3134−3143.

(44) Mitchell, M. *Engauge Digitizer*, version 2.12 (free software available from http://digitizer.sourceforge.net under the GNU General Public License (Version 2)).

(45) Bibo, A. M.; Knobler, C. M.; Peterson, I. R. *J. Phys. Chem.* **1991**, *95*, 5591−5599.

(46) Grimmett, G. *Percolation*, 2nd ed.; Springer-Verlag: New York, 1999.

(47) Stauffer, D.; Aharony, A. *Introduction to percolation theory*, 2nd ed.; Taylor & Francis: Washington, DC, 1992.

(48) Jacobs, D. J.; Thorpe, M. F. *Phys. Rev. Lett.* **1995**, *75*, 4051−4054.

(49) Jacobs, D. J.; Thorpe, M. F. *Phys. Rev. E* **1996**, *53*, 3682−3693.

(50) Bringezu, F.; Ding, J. Q.; Brezesinski, G.; Zasadzinski, J. A. *Langmuir* **2001**, *17*, 4641−4648.

(51) Ding, J.; Warriner, H. E.; Zasadzinski, J. A. *Phys. Rev. Lett.* **2002**, *88*, 168102-4.

(52) Alonso, C.; Alig, T.; Yoon, J.; Bringezu, F.; Warriner, H.; Zasadzinski, J. A. *Biophys. J.* **2004**, *87*, 4188−4202.

(53) McConnell, H. M.; Radhakrishnan, A. *Biochim. Biophys. Acta* **2003**, *1610*, 159−173.

(54) Ege, C.; Ratajczak, M.; Majewski, J.; Kjaer, K.; Lee, K. Y. C. *Biophys. J.* **2006**, *91*, L01−L03.

(55) Keller, S. L.; Radhakrishnan, A.; McConnell, H. M. *J. Phys. Chem. B* **2000**, *104*, 7522−7527.

(56) Radhakrishnan, A.; McConnell, H. M. *Biophys. J.* **1999**, *77*, 1507−1517.

(57) Okonogi, T. M.; McConnell, H. M. *Biophys. J.* **2004**, *86*, 880−890.

(58) Sacre, M. M.; Tocanne, J. F. *Chem. Phys. Lipids* **1977**, *18*, 334−354.

(59) Helm, C. A.; Laxhuber, L.; Lösche, M.; Möhwald, H. *Colloid Polym. Sci.* **1986**, *264*, 46−55.

(60) Grigoriev, D.; Krustev, R.; Miller, R.; Pison, U. *J. Phys. Chem. B* **1999**, *103*, 1013−1018.

(61) Johann, R.; Vollhardt, D.; Möhwald, H. *Langmuir* **2001**, *17*, 4569−4580.

(62) McConlogue, C. W.; Vanderlick, T. K. *Langmuir* **1999**, *15*, 234−237.

(63) Kruger, P.; Losche, M. *Phys. Rev. E* **2000**, *62*, 7031−7043.

(64) Kooijman, E. E.; Chupin, V.; Fuller, N. L.; Kozlov, M. M.; de Kruijff, B.; Burger, K. N. J.; Rand, P. R. *Biochemistry* **2005**, *44*, 2097−2102.

(65) Israelachvili, J. N. *Intermolecular and Surface Forces*, 2nd ed.; Academic Press: San Diego, CA, 1992.

(66) Zhang, Y.; Fischer, T. M. *J. Phys. Chem. B* **2005**, *109*, 3442−3445.

(67) Kato, T. *Langmuir* **1990**, *6*, 870−872.

(68) Gourier, C.; Knobler, C. M.; Daillant, J.; Chatenay, D. *Langmuir* **2002**, *18*, 9434−9440.

(69) Crane, J. M.; Hall, S. B. *Biophys. J.* **2001**, *80*, 1863−1872.

(70) Toninelli, C.; Biroli, G.; Fisher, D. S. *Phys. Rev. Lett.* **2006**, *96*, 035702-4.

(71) Monroy, F.; Ortega, F.; Rubio, R. G.; Ritacco, H.; Langevin, D. *Phys. Rev. Lett.* **2005**, *95*, 056103.

(72) Notter, R. H. *Lung surfactants: basic science and clinical applications; Lung biology in health and disease*; Marcel Dekker: New York, 2000; Vol. 149.

(73) Tanaka, Y.; Takei, T. *Chem. Pharm. Bull.* **1983**, *31*, 4091−4099.

(74) Tanaka, Y.; Takei, T.; Kanazawa, Y. *Chem. Pharm. Bull.* **1983**, *31*, 4100−4109.

(75) Tanaka, Y.; Takei, T.; Masuda, K. *Chem. Pharm. Bull.* **1983**, *31*, 4110−4115.